Evaluation of urinary bladder fibrogenesis in a mouse model of long-term ketamine injection

CHENG-HUANG SHEN[1*], SHOU-CHIEH WANG[2*], SHOU-TSUNG WANG[3,4], SHU-MEI LIN[4], JIANN-DER WU[5], CHANG-TE LIN[1] and YI-WEN LIU[3]

[1]Department of Urology, Chiayi Christian Hospital, Chiayi 600; [2]Division of Nephrology, Department of Internal Medicine, Kuang Tien General Hospital, Taichung 437; [3]Department of Microbiology, Immunology and Biopharmaceuticals; [4]Department of Food Science, College of Life Sciences, National Chiayi University; [5]Department of Pathology, Chiayi Christian Hospital, Chiayi 600, Taiwan, R.O.C.

Received July 4, 2015; Accepted June 22, 2016

DOI: 10.3892/mmr.2016.5482

Abstract. Long-term ketamine abuse has been shown to affect the lower urinary tract and result in interstitial cystitis-like syndrome. However, the causative mechanism of ketamine-induced dysfunction remains unclear. The present study aimed to investigate the physiological, histological and molecular changes on ketamine-associated cystitis (KC) in a mouse model. Both male and female Balb/c mice were separately distributed into the control group (normal saline) and ketamine group, which received ketamine hydrochloride (100 mg/kg/day) daily by intraperitoneal injection for a total period of 20 weeks. In each group, the urine was analyzed by gas chromatography-mass spectrometry to measure the concentration of ketamine and its metabolites. Urinary frequency and urine volume were examined to investigate the urinary voiding functions. Mice bladders were excised for cDNA microarray and hematoxylin and eosin (HE) staining. The ketamine and metabolites were detected only in ketamine-treated mice urine. The voiding interval was reduced in the male mice group after 20 week ketamine administration. Additionally, the result of cDNA array analysis revealed a number of gene expression levels involved in chronic wound healing response and collagen accumulation, which were closely associated with fibrosis progression in the connective tissue. In HE staining of the bladder tissue, the ketamine-injected mice exhibited prominently denser blood vessel distribution in the submucosal layer. Based on the evidence in the present study, a mechanism that delineates fibrosis formation of urinary bladder induced by the pathogenesis of ketamine abuse can be constructed.

Correspondence to: Professor Yi-Wen Liu, Department of Microbiology, Immunology and Biopharmaceuticals, College of Life Sciences, National Chiayi University, 300 Syuefu Road, Chiayi 600, Taiwan, R.O.C.
E-mail: ywlss@mail.ncyu.edu.tw

*Contributed equally

Abbreviations: DEG, differentially expressed genes; GC-MS, gas chromatography-mass spectrometry; GO, gene ontology; HE stain, hematoxylin and eosin stain; KEGG, Kyoto encyclopedia of genes and genomes; MOA, mouse oligonucleotide DNA microarray; VSOP, voided stain on paper

Key words: angiogenesis, collagen, fibrosis, ketamine-induced cystitis, ketamine, urinary bladder

Introduction

Ketamine, a clinical anesthesia, was first synthesized in 1961 (1). Recently, ketamine has become an increasingly popular recreational drug used illicitly by people in clubs or the younger generation. Since the first two clinical case reports about ketamine abuse-induced urological sequelae were published in 2007 (2,3), it has been well-known that long-term ketamine abuse causes side effects that resemble ketamine-associated cystitis (KC), which is associated with severe lower urinary tract symptoms, including smaller bladder capacity, incontinence, dysuria, and hematuria, as well as lower abdominal or suprapubic pain resulting from neurological disorders (4).

To date, the underlying mechanisms of ketamine-induced urinary toxicity remain to be completely understood. However, several hypotheses on the association between ketamine and urinary tract damage have been raised based on clinical observations. The most straightforward and important one points out that ketamine and its metabolites in the urine may have a direct toxic effect on the bladder urothelium, leading to a chronic inflammatory response and subsequent interstitial cystitis-like symptoms (4). In addition, numerous previous studies using rodents for investigating the mechanisms of KC have been reported (5-11). According to the outcome of these previous studies, certain characteristics, such as submucosal infiltration of mononuclear inflammatory cells (5,6) and gene expression, including cyclooxygenase (COX)-2 and inducible nitric oxide synthase (iNOS) (5,7), can link to submucosa inflammatory environment caused by ketamine abuse in clinical cases. Other evidence associated with detrusor over-activity comes from the increase of adenosine triphosphate-evoked detrusor contraction and P2X1 receptor protein observed in Meng *et al* (8).

Alternatively, in Gu's rat model (9), the phosphorylated transgelin of the bladder smooth muscles was increased by ketamine treatment, suggesting that transgelin may have a role in modulating bladder detrusor contractility. Previously, an innovative technique using TGF-β1 injection has also been successfully generated in a reproducible rat model to assess urethral fibrosis (10).

In our previous microarray study, in which male Balb/c mice received 30 mg/kg/day ketamine injection for 2 months, the gene expression of keratin 14, which assembles with keratin 5 to form heterodimers and contribute to the intermediate filament cytoskeleton, was found to markedly decrease in the urothelial tissue (11). This result revealed that the urothelial cells possibly suffered damage from ketamine and likely progressed to a leaked barrier or denuded condition. Therefore, based on the theory of urothelial pathogenesis, it is reasonable to illustrate the effectiveness of intravesical therapy with hyaluronic acid in ketamine-abused patients (12). However, in that study, hematoxylin and eosin (HE) stain analysis revealed no histological difference between the bladders of the control and ketamine-treated mice. Therefore, in the design of the present study, enhanced ketamine dosage (100 mg/kg/day) and prolonged injection period (20 weeks) were administered for both male and female Balb/c mice in order to search for advanced markers associated with the pathogenesis of KC.

Materials and methods

Animals and ketamine treatment. Male and female (n=20 each) 6-week-old Balb/c mice were purchased from the National Laboratory Animal Center (Taipei, Taiwan). All animals were maintained at the qualified animal care facility of Biotechnology and Health Hall in National Chiayi University (Chiayi, Taiwan) for a 1 week period of acclimation. At 7 weeks of age, 10 male and 10 female mice were administered 100 mg/kg ketamine (Merial Laboratoire de Toulouse, Lyon, France) via intraperitoneal injection daily for 20 weeks. A control group of 10 male and 10 female mice were injected with normal saline. All mice were housed in polycarbonate cages, provided with food and water *ad libitum* and maintained on a 12 h light-dark cycle at 22±2˚C. The animal experiment was approved by the Institutional Animal Care and Use Committee of National Chiayi University (no. 102029).

Detection of ketamine and its metabolites in mice urine using gas chromatography-mass spectrometry (GC-MS). Urine was collected three days prior to the final day of the 20th week. Ketamine and its metabolites were excreted primarily by the kidney, with an elimination half-life of around 2 h in rats (13). The urine from six mice from each group was collected together during a period of 30 min to 4 h following intraperitoneal injection to analyze the concentration of ketamine and its metabolites (norketamine and dehydronorketamine). The collected urine was first filtered using the ultrafiltration Vivaspin 500 device (GE Healthcare Life Sciences, Little Chalfont, UK) with 3 kDa molecular weight cut off achieved by centrifuging at 9,700 x g at 4˚C for 30 min. The concentration of ketamine and its metabolites were determined using modified liquid-liquid [triethylamine:cyclohexane, 3:1 (v/v)] extraction, accompanied by GC-MS on a Shimadzu GCMS-QP2010 system (14). The gas chromatograph was equipped with a 30-m DB-5MS (J&W Scientific, Folsom, CA, USA) capillary column with 250 μm I.D. and 0.25 μm film thickness. The injector temperature and GC-MS interface temperature were maintained at 220 and 280˚C, respectively. The sample was delivered in splitless mode and the helium carrier gas flow rate was 0.8 ml/min. The temperature of the GC oven was set at 100˚C for 0.5 min, then increased to 280˚C at 25˚C/min and held for 1 min.

Mouse voiding behavior analysis. This analysis was made one day prior to the final day of the 20th week. Urinary voiding quantity and interval were determined using the voided stain on paper (VSOP) method (15). Briefly, the mice were fed with 20 μl/g distilled water. Following waiting for 30 min, the mice were placed on a 25 cm wire-netted grid above a filter paper (Advantec 185 mm; Tokyo Roshi Kaisha, Ltd., Tokyo, Japan). Each mouse was restricted in a certain area matched to a filter paper. Subsequently the voiding time and area were recorded over 2 h. The recorded urine stains were scanned into image files and the stained areas were calculated using the software ImageJ v1.47 (National Institutes of Health, Bethesda, MA, USA). Each voiding interval was calculated based on the time difference between two near voiding episodes. The voiding interval of an individual mouse was the mean of all voiding intervals within a 2 h period.

Mice bladder collection, histological stains and total RNA extraction. Following treatment for 20 weeks, the mice were euthanized by carbon dioxide inhalation and the bladders were removed. A total of 24 bladders (n=6/group) were fixed in 10% neutral formalin for 24 h and then embedded in paraffin and cut into 3 μm sections for preparation of slides used in follow-up histological analysis, which includes HE stain for microvascular location purposes, as well as Masson's trichrome stain to identify collagen distribution. Following staining, these tissue sections were subsequently examined by light microscopy. Furthermore in each group, 2-4 urinary bladders were homogenized individually and the total RNA was extracted using the TRIzol reagent (Thermo Fisher Scientific, Inc., Waltham, MA, USA), according to the manufacturer's instructions. The concentration and purity of the RNA was measured using a NanoDrop 1000 spectrophotometer (Thermo Fisher Scientific, Inc.). Purity was checked using the ratio of the OD_{260}/OD_{280} and OD_{260}/OD_{230}. The quality of total RNA was accessed using Agilent 2100 Bioanalyzer (Agilent Technologies, Inc., Santa Clara, CA, USA).

Mouse oligonucleotide DNA microarray. The Mouse Whole Genome OneArray® v2 (Phalanx Biotech Group, Hsinchu, Taiwan) contains 27,307 DNA oligonucleotide probes. Each probe is a 60-mer designed in the sense direction. Among the probes, 26,423 probes correspond to the annotated genes in RefSeq v42 (ftp://ftp.ncbi.nlm.nih.gov/refseq/release/release-catalog/archive/release42.files.installed) and Ensembl v59 databases (ftp://ftp.ensembl.org/pub/release-59/fasta/mus_musculus/cdna/Mus_musculus.NCBIM37.59.cdna.all.fa.gz). In addition, 884 control probes were also included. The detailed descriptions of the gene array list are available from http://www.phalanx.com.tw/products/MOA.php.

Table I. Concentration of ketamine and its metabolites in mice urine.

Gender	K (ppm)	NK (ppm)	deNK (ppm)
Female	108±9.9	336±17.1	1,332±66.0
Male	173±9.1	599±8.4	1,286±13.7

The data are presented as the mean ± standard deviation. K, ketamine; NK, norketamine; deNK, dehydronorketamine.

Microarray analysis. Fluorescent aRNA targets were prepared from 1 μg total RNA samples using OneArray® Amino Allyl aRNA Amplification kit (Phalanx Biotech Group) and Cy5 dye (GE Healthcare Life Sciences). Fluorescent targets were hybridized to the Mouse Whole Genome OneArray® with Phalanx hybridization buffer using Phalanx Hybridization system. After 16 h hybridization, non-specific binding targets were removed using saline and sodium citrate buffer. The slides were scanned using a DNA Microarray Scanner (Model G2505C; Agilent Technologies, Inc.). The Cy5 fluorescent intensities of each spot were analyzed using GenePix 4.1 software (Molecular Devices, LLC, Sunnyvale,. CA, USA). Each single sample was at least assessed twice in terms of technical or biological replicates under the reproducibility >0.975. The signal intensity was loaded into Rosetta Resolver system® (Rosetta Biosoftware, Seattle, WA, USA) for data pre-processing and 75 percentile centering normalization was applied. The errors of the sample were estimated by using the error-weighted approach at the same time. The fold change and P-value for pair-wise sample comparison were calculated for evaluating differentially expressed genes (DEGs). The criteria with $\log_2|\text{fold change}| \geq 0.5$ and $P<0.05$ were used for further analysis.

Reverse transcription-quantitative polymerase chain reaction (RT-qPCR) analysis. In the present study, two genes [Collagen α-1 (III) chain (Col3a1) and Collagen α-2 (I) chain (Col1a2)] were selectively targeted. Each reaction included 20 ng cDNA, 500 nM forward and reverse primers, and 2X Fast SYBR Green PCR Master mix (Applied Biosystems; Thermo Fisher Scientific, Inc.). A total of 10 μl reaction volumes were used for qPCR with the specific primers listed as follows: Col1a2, forward: 5'-TGGCTTCTGACTATCTTCCACAG-3' and reverse: 5'-CAGTTCGTGTCAGCCTTGGT-3'; Col3a1, forward: 5'-GCAACGGTCATACTCATTCACC-3' and reverse: 5'-GTTCTGACCAGTTGAGGTAGTT-3'; Actb reference gene, forward: 5'-GTCCACCTTCCAGCAGATGT-3' and reverse: 5'-CTCAGTAACAGTCCGCCTAGAA-3'. Each sample was tested in triplicate. The Bio-Rad CFX Connect (Bio-Rad Laboratories, Inc., Hercules, CA, USA) real-time PCR machine and Bio-Rad CFX Manager version 3.0 software (Bio-Rad Laboratories, Inc.) were used for the experimental setup and data analysis. The qPCR data of the target genes were normalized against the reference gene, Actb.

Gene pathway building. To interpret the biological functions of the DEGs between the control and ketamine-treated groups, Gene Ontology (GO) enrichment analysis was used to explore the functional distribution. Additionally, the Kyoto Encyclopedia of Genes and Genomes (KEGG) database was applied to analyze the DEGs to identify essential pathways involved in the microarray data.

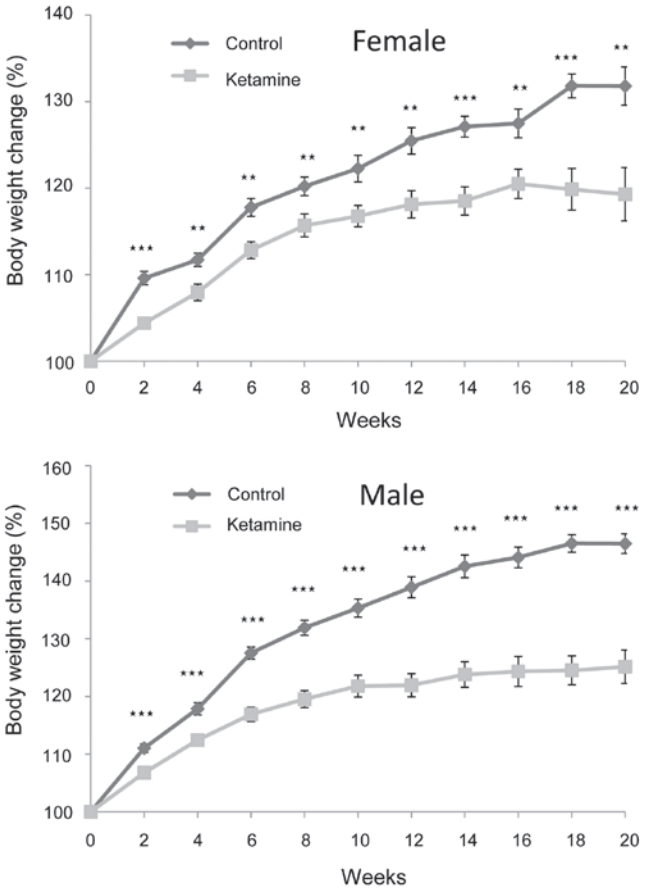

Figure 1. Changes in the body weight of the mice. The weight growth of the ketamine-treated mice was significantly less compared with that of controls after the 2 week treatment. The data are presented by the mean ± standard error of the mean (**P<0.01; ***P<0.001 compared with the control).

Statistical analysis. Statistical differences were analyzed using one-way analysis of variance analysis, with the exception of the microarray data. All statistics were calculated using SigmaPlot version 12.5 (Systat Software, Inc., San Jose, CA, USA). Data are presented as the mean ± standard error of the mean with the exception of data in Table I, which are expressed as the mean ± standard deviation. $P<0.05$ was considered to indicate a statistically significant difference.

Results

Effect of ketamine on mouse behavior and body weight. At the dosage of 100 mg/kg/day, it was found that the mice at first displayed excitation within 1 min following ketamine injection. They gradually turned into anesthetic status in ~2 min and lasted for ~30 min. In awakening from the anesthesia, the mice first entered a semi-conscious state for ~10 min and then became fully awake. The rate of weight gain of the ketamine-treated mice became significantly slower following the second week compared with that of the control mice. This

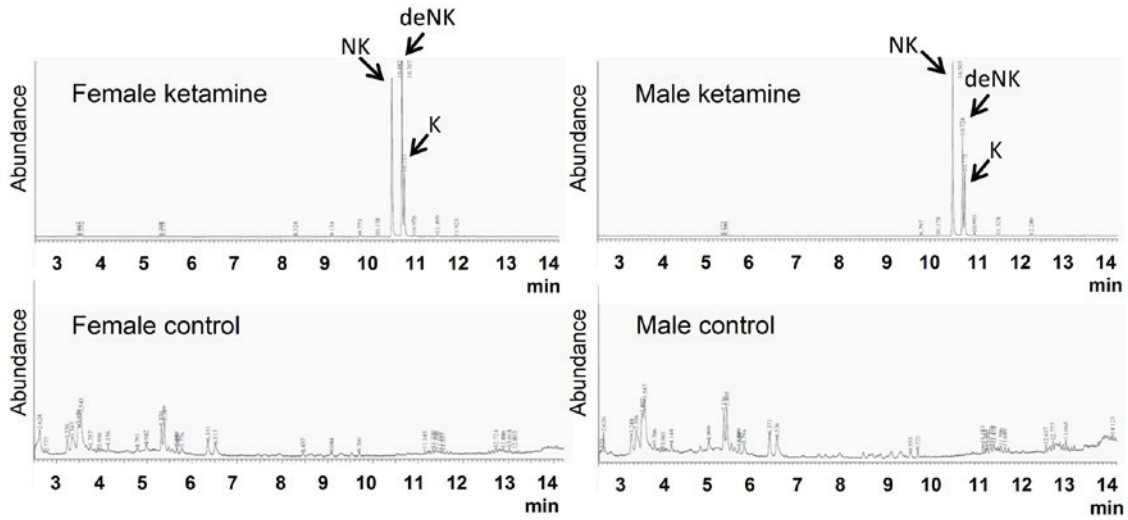

Figure 2. A typical total ion current chromatogram derived from the extracted mice urine. The total run time was 14 min. Ketamine and its metabolites appeared around 10-11 min following the order of NK, deNK and K. No detected level was observed in both male and female control groups. NK, norketamine; deNK, dehydronorketamine; K, ketamine.

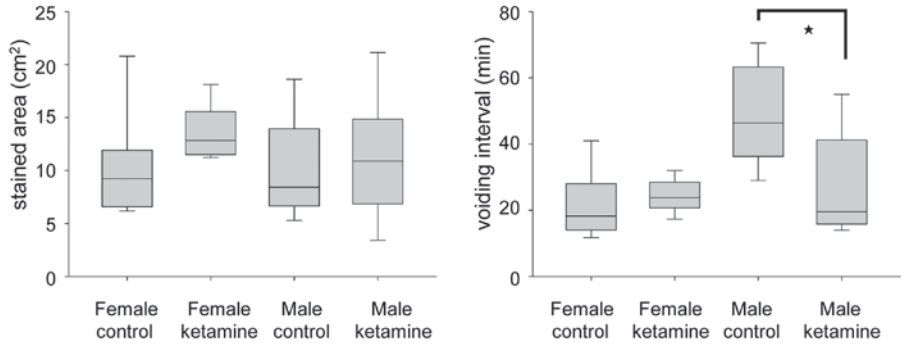

Figure 3. Voiding quantity and frequency of the mice. The data were recorded following voided stain on paper method at week 20 (n=8 for each group). *P<0.05.

trend continued for the remaining period of the present study (Fig. 1). Additionally, male mice were more obvious than female mice in this regard, indicating that ketamine toxicity likely caused more severe physiological effects on the male mice.

Ketamine concentration and its metabolites in mice urine. The concentrations of ketamine and ketamine metabolites (norketamine and dehydronorketamine) in urine were detected by GC-MS. These three types of urinary concentrations were undetectable in the control groups (Fig. 2). Following calculation using three individual standard curves, the concentrations of ketamine, norketamine and dehydronorketamine in mice urine were determined (Table I). The concentrations of ketamine metabolites were markedly higher compared with the original form of ketamine, which implied that the urinary toxic effects of ketamine may result from the large quantities of ketamine metabolites in the urine.

Effect of ketamine in the voiding behavior of mice. The voiding quantity and micturition interval were recorded within 2 h using the VSOP method. At week 20, the voiding interval of ketamine-treated male mice was found to be significantly smaller compared with that of control male mice, while no change was observed in the female group (Fig. 3). These results indicated that ketamine toxicity may be more serious in male mice under long-term ketamine influence. This phenomenon appeared consistent with the weight loss of the ketamine-treated male mice, which was more apparent compared with that of the ketamine-treated female mice.

DEGs and pathways identified through microarray analysis of mice bladder tissue. To determine the genes and pathways involved in ketamine-induced toxicity on urinary bladder, the total RNA was extracted from the bladders of the 20 week ketamine-treated mice and of the control mice. The bladdes were subsequently analyzed on the Mouse Whole Genome OneArray® v2 microarray chip containing 27,307 probes. The whole microarray data has been deposited in the GEO database (accession number, GSE68539). The standard selection criteria used to identify the DEGs were $\log_2$|fold change| ≥0.5 and P<0.05. The male and female mice data were normalized respectively and were included together to do the further calculation. Compared with the control group, 44 upregulated DEGs and 70 downregulated DEGs were identified for the ketamine-treated mice. To interpret the biological functions of

Table II. Top 15 enriched GO terms of DEGs.

Male mice			Female mice		
Gene set name	No. genes	P-value	Gene set name	No. genes	P-value
Molecular functions					
Receptor binding	10	6.34E-06	DNA binding	15	3.29E-06
Transmembrane receptor activity	10	1.55E-05	Enzyme binding	8	1.12E-05
Purine ribonucleotide binding	7	3.29E-05	Identical protein binding	10	1.42E-05
Chemokine receptor binding	4	3.62E-05	Receptor binding	11	1.62E-05
Purine nucleotide binding	7	3.95E-05	Phosphoric ester hydrolase activity	7	3.57E-05
Receptor activity	11	5.12E-05	Ion binding	9	3.75E-05
Transcription repressor activity	6	5.45E-05	Cation binding	8	4.07E-05
Identical protein binding	8	5.73E-05	Transcription factor activity	10	5.15E-05
Nucleotide binding	7	5.76E-05	Protein kinase activity	9	5.22E-05
Adenyl ribonucleotide binding	6	8.03E-05	Protein homodimerization activity	6	8.33E-05
Enzyme regulator activity	8	8.74E-05	Hormone activity	4	1.30E-04
G protein coupled receptor binding	4	8.93E-05	Phosphotransferase activity alcohol group as acceptor	9	1.73E-04
Adenyl nucleotide binding	6	9.80E-05	Receptor activity	12	1.91E-04
Carbohydrate binding	4	2.73E-04	Hydrolase activity acting on ester bonds	8	2.04E-04
Glycosaminoglycan binding	3	4.27E-04	Purine ribonucleotide binding	7	2.22E-04
Biological process					
Signal transduction	39	2.71E-18	Signal transduction	42	8.98E-16
Muticellular organismal development	27	1.23E-13	Multicellular organismal development	31	2.02E-13
Response to external stimulus	14	1.10E-10	Biopolymer metabolic process	38	1.30E-12
Negative regulation of biological process	19	1.54E-10	Positive regulation of cellular process	24	2.19E-12
Cell cell signaling	15	3.25E-10	Positive regulation of biological process	24	7.58E-12
Negative regulation of cellular process	18	5.37E-10	Negative regulation of biological process	23	1.96E-11
System development	20	1.31E-09	Negative regulation of cellular process	22	5.22E-11
Anatomical structure development	21	3.69E-09	Protein metabolic process	30	5.87E-11
System process	16	3.85E-09	System development	25	7.10E-11
Intracellular signaling cascade	17	6.20E-09	Anatomical structure development	27	8.01E-11
Immune system process	12	2.70E-08	Cellular protein metabolic process	28	1.42E-10
Regulation of biological quality	13	4.21E-08	Cellular macromolecular metabolic process	28	1.88E-10
Behavior	8	3.74E-07	Regulation of biological quality	17	6.30E-10
Second messenger mediated signaling	8	3.74E-07	Cell development	19	1.94E-09
Response to stress	13	3.82E-07	Biopolymer modification	20	2.29E-09

SPANDIDOS PUBLICATIONS
MOLECULAR MEDICINE REPORTS 14: 1880-1890, 2016

Table II. Continued.

Male mice			Female mice		
Gene set name	No. genes	P-value	Gene set name	No. genes	P-value
Cellular component					
Extracellular region	15	1.29E-09	Membrane	46	1.77E-15
Membrane	30	2.67E-09	Cytoplasm	47	4.46E-15
Intrinsic to membrane	23	2.39E-08	Membrane part	36	1.94E-11
Membrane part	25	7.07E-08	Plasma membrane	32	1.04E-10
Integral to membrane	22	8.43E-08	Cytoplasmic part	30	9.19E-10
Plasma membrane	22	2.76E-07	Integral to membrane	28	6.61E-09
Extracellular region part	11	2.96E-07	Intrinsic to membrane	28	8.80E-09
Plasma membrane part	18	3.20E-06	Extracellular region	15	7.94E-08
Cytoplasm	25	5.86E-06	Plasma membrane part	24	1.12E-07
Integral to plasma membrane	15	2.51E-05	Intracellular organelle part	23	7.14E-07
Intrinsic to plasma membrane	15	2.95E-05	Organelle part	23	7.67E-07
Extracellular space	7	1.01E-04	Macromolecular complex	19	3.79E-06
Collagen	3	1.31E-04	Nucleus	24	4.51E-06
Cytoplasmic part	16	3.55E-04	Extracellular region	11	5.85E-06
Golgi apparatus	6	4.58E-04	Nuclear part	13	4.36E-05

GO, gene ontology; DEG, differentially expressed genes.

Table III. Enriched KEGG pathway of DEGs.

KEGG pathway	No. genes	P-value
Male mice		
Focal adhesion	7	1.52E-05
MAPK signaling	7	9.17E-05
Chemokine signaling	5	9.28E-04
ECM receptor interaction	5	2.04E-05
p53 signaling	5	7.78E-06
Vascular smooth muscle contraction	5	9.20E-05
Prion disease	4	1.06E-05
TOLL-like receptor signaling	4	7.02E-04
ABC transporters	3	6.84E-04
Sphingolipid metabolism	3	5.16E-04
Female mice		
Cytokine-cytokine receptor interaction	10	1.27E-06
Pathways in cancer	9	5.08E-05
Dilated cardiomyopathy	7	4.78E-07
MAPK signaling	7	4.58E-04
Chemokine signaling	6	4.42E-04
Endocytosis	6	3.63E-04
Arrhythmogenic right ventricular Cardiomyopathy	5	4.42E-05
Hypertrophic cardiomyopathy	5	7.57E-05
Oocyte meiosis	5	3.01E-04
p53 signaling	4	4.30E-04

KEGG, Kyoto encyclopedia of genes and genomes; DEG, differentially expressed gene; MAPK, mitogen-activated protein kinase; ECM, extracellular matrix.

the DEGs, GO enrichment analysis, which provides a common descriptive framework and functional annotation of gene sets data, was performed to examine the functional distributions and classification of the gene sets belonging to male and female mice individually. The GO categories were separated into three groups: Biological process, cellular component and molecular function. The top 15 enriched GO terms of the three categories are shown in Table II. The GO enrichment analysis revealed that genes coding for signaling transduction, likely concerned with the extracellular matrix (ECM) components and cell membrane receptors, serve relevant roles. KEGG pathway enrichment analysis was also performed to identify the essential pathways. From the results, cytokine/chemokine- and ECM function-associated information were much more prominent (Table III).

Expression changes of genes associated with fibrosis. After checking the essential DEGs in detail, the present study listed certain critical genes that are all associated with connective tissue fibrogenesis (Table IV). Notably among them, two collagen genes, Col3a1 and Col1a2 that encoded proteins highly associated with bladder fibrotic diseases (16), were upregulated. Additionally, the remaining genes obviously served as growth factors [e.g. Amphiregulin (Areg)], cytokines/chemokine [e.g. C-C chemokine receptor type (Ccr)2 and Chemokine (C-C motif) ligand (Ccl)7], or that they serve a role in cell mobility [e.g. Collagen triple helix repeat containing 1 (Cthrc1)], ECM remodeling [e.g. A disintegrin-like and metallopeptidase with thrombospondin type 1 motif, (Adamts)1] or angiogenesis [e.g. Platelet/endothelial cell adhesion molecule (Pecam)1 and endothelin 1], which were all directly or indirectly involved in the progression of wound healing and development into plausible chronic fibrosis. Taken together, the presence of type I and III collagens accumulating together with the DEGs in Table IV is highly indicative of the tendency for fibrogenesis and may have a marked association with the effects of ketamine. Furthermore, the expression levels of Col3a1 and Col1a2 were confirmed by RT-qPCR, which was consistent with the microarray data and revealed that ketamine treatment increased their gene expression levels (Fig. 4).

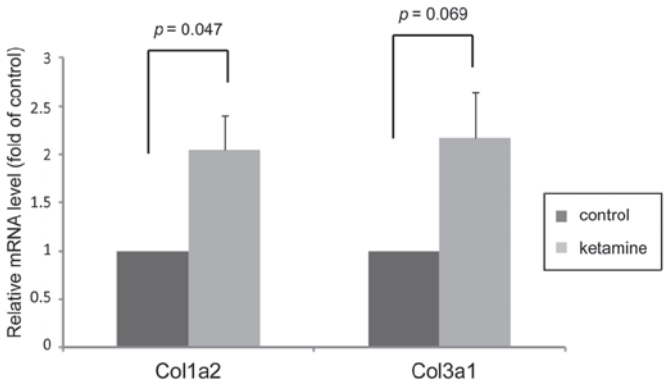

Figure 4. Reverse transcription-quantitative polymerase chain reaction of two upregulated collagen genes. The mRNA samples extracted from four control and three ketamine group mice were assessed. The relative expression value of a gene was normalized against the expression of Actb from mice mRNA at week 20. The data are presented by the mean ± standard error of the mean.

Effect of ketamine in bladder angiogenesis and fibrosis by histopathological analysis. Since two angiogenesis-associated genes were found to be upregulated in the result of microarray analysis, the bladder HE stain was used to confirm the vessel distribution. When compared with the control mice, the ketamine-injected mice exhibited prominently denser blood vessel distribution in the submucosal layer (Fig. 5). According to the increase in blood vessel number, it fits with the biological results of angiogenic factors found in the DEGs of the present microarray data. The present study also verified the collagen density by Masson's trichrome stain analysis (Fig. 6). However, it revealed no obvious increase of collagen accumulation in the submucosa region between the ketamine-treated with control groups due to the similar ratio calculated using ImageJ from connective tissue area relative to muscle tissue or urothelial layer area (data not shown). This result indicated that the progression of fibrogenesis likely remained at the initial stage.

Discussion

In the present study, a 20 week ketamine-injection mouse model was used to characterize the effects of long-term ketamine abuse on bladders by examining critical changes

Table IV. Potential DEGs involved in fibrogenesis of ketamine-treated mice.

Gene ID	Gene symbol	Official full name	Fold change	P-value
57266	Cxcl14	Chemokine (C-X-C motif) ligand 14	-0.787	9.49E-06
11687	Alox15	Arachidonate 15-lipoxygenase	-0.684	2.66E-03
59289	Ccbp2	Chemokine binding protein 2	-0.620	7.91E-05
12772	Ccr2	Chemokine (C-C motif) receptor 2	0.939	1.05E-01
20306	Ccl7	Chemokine (C-C motif) ligand 7	0.820	1.04E-01
12825	Col3α1	Collagen, type III, α1	0.676	2.35E-03
11839	Areg	Amphiregulin	0.664	1.42E-02
12843	Col1α2	Collagen, type I, α2	0.654	4.06E-04
68588	Cthrc1	Collagen triple helix repeat containing 1	0.609	2.25E-02
13614	Edn1	Endothelin 1	0.595	1.04E-02
11504	Adamts1	A disintegrin-like and metallopeptidase with thrombospondin type 1 motif, 1	0.548	5.84E-03
12832	Col5α2	Collagen, type V, α2	0.521	2.43E-02
18613	Pecam1	Platelet/endothelial cell adhesion molecule 1	0.517	1.10E-02

The fold change value is adopted by log2. DEG, differentially expressed gene.

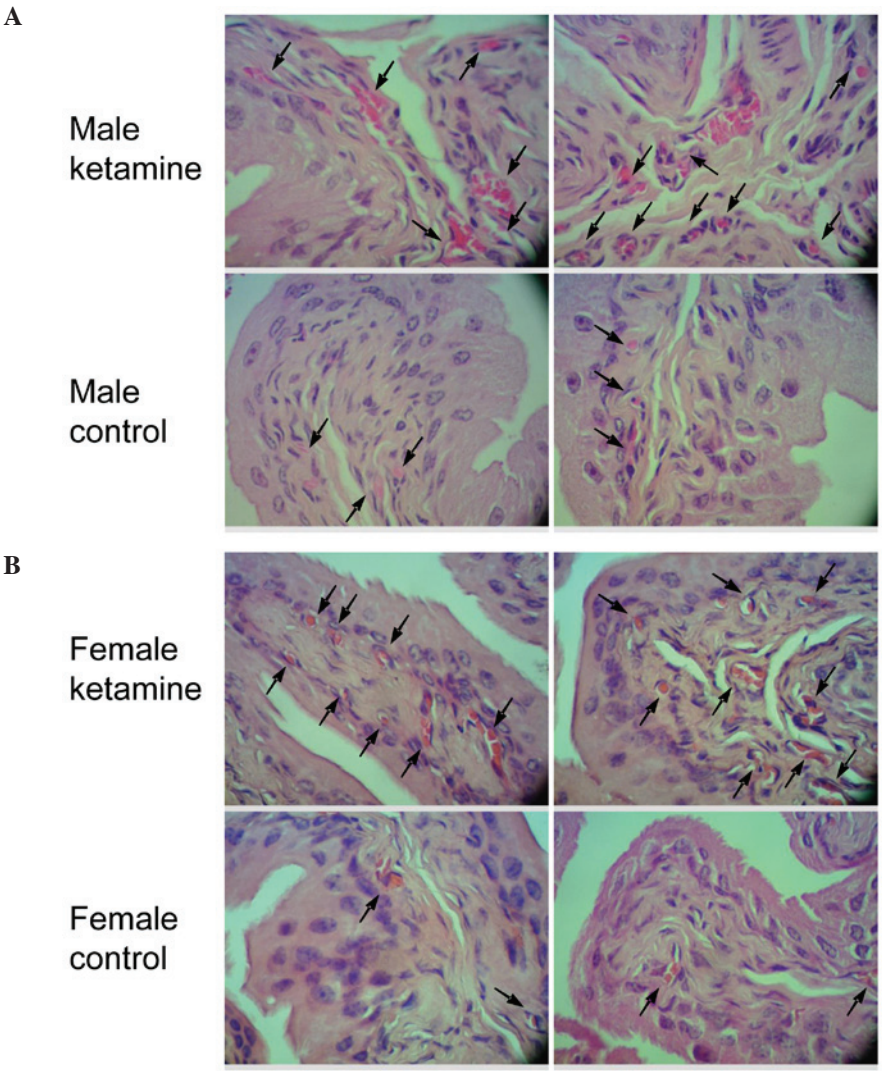

Figure 5. HE staining images of the mice bladders. The ketamine-injected mice exhibited denser blood vessel distribution compared with the controls in (A) male and (B) female mice. The black arrows point the blood vessels. Images of the HE stained bladder tissues were captured by microscopy (magnification, x400). HE, hematoxylin and eosin.

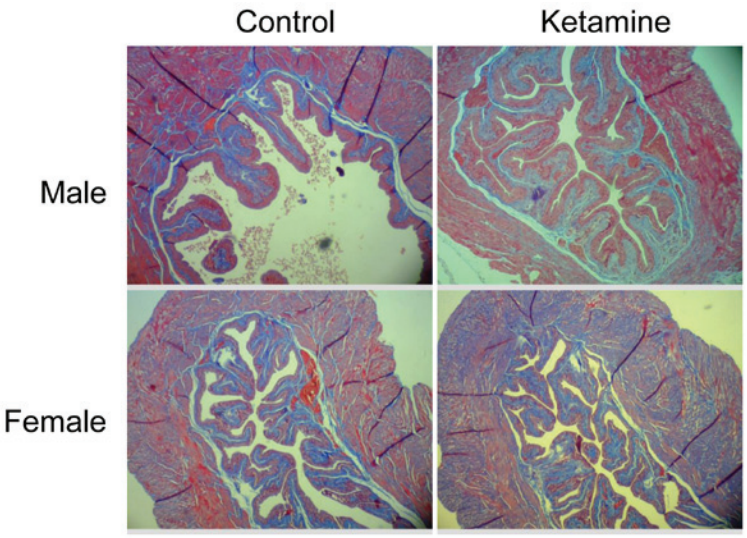

Figure 6. Masson's trichrome staining images of the mice bladders. The ketamine-injected mice exhibited no significant difference in the distribution of collagen proteins compared with the controls. Images of the bladder tissue were captured by microscopy (magnification, x40).

of gene expression. The aim was to explore the mechanisms for clinical management or therapeutic development. Through GC-MS quantification, high concentrations of ketamine and its metabolites were present in mice urine following injection (Table I and Fig. 2). In addition, after 2 weeks of ketamine treatment, the body weight of the ketamine-treated group was significantly lower compared with the control mice. This phenomenon may result from reduced food consumption, similar to the loss of appetite and weight shown in human abusers (17), as well as in animals (8). Additionally, the presence of decreased body weight may likely reflect the physiological stress suffered from ketamine treatment. Notably, the body weight loss and voiding behavior change in the ketamine-treated male mice were more obvious compared with that in female mice. This result may be associated with the higher concentration of ketamine and norketamine measured in the urine of male group (Table I). However, other factors related to mouse gender, including the difference in hormone or metabolic enzymes, may also serve a role and require future investigation. In addition, from the microarray analysis, the most obvious clues come from the upregulated type I (Col1a2) and III (Col3a1) collagens (Table IV and Fig. 4), since their enriched transcription has been considered sensitive markers of active fibrogenesis (18,19). To date, the pathological cause of fibrosis affected by ketamine toxicity remains to be completely elucidated.

In general, fibrosis originates from an abnormal wound healing process in which tissue repair is deregulated as a result of excessive ECM accumulation. According to the classical model of wound healing, the cellular course of events can be divided into certain sequential, yet overlapping phases, including inflammatory, proliferative and tissue remodeling stages (20,21). During the proliferation phase in particular, if the production of pro-inflammatory cytokines/chemokines and growth factors by parenchymal cells is persistent, the ongoing ECM production will eventually destroy the normal balance between collagen formation and degradation (22). In this context, it was revealed that several chemokines and corresponding receptor, including Ccr2, Ccl7 and Ccbp2, were involved (Table IV). Ccr2 has been reported to initiate the fibrotic environment in the liver and lung (23,24). Similarly, overexpressed Ccl7 in fibroblasts also contributes to excessive accumulation of the ECM (25). By contrast, Ccbp2 is hypothesized to act as a chemokine scavenger to counteract the function of Ccl2 (26). Notably, the expression of Ccbp2 simultaneously decreased in the present results. Additional clues come from the increased expression of growth factor-like molecule endothelin-1, since accumulating evidence has suggested that endothelin-1 would result in fibrogenesis via an autocrine loop (27), which drives fibroblast activation, proliferation, as well as differentiation into myofibroblasts thus leading to excessive collagen deposition (28). Another pivotal anti-fibrotic factor, Alox15, which is the key enzyme for the synthesis of lipoxins, can counteract fibroblast activation and experimental fibrosis (29). Notably, in the present data, Alox15 remains on the negative expression list.

Wound healing is a dynamic and complex process that requires cooperative regulation of angiogenesis and cell migration capacity (20). Angiogenesis is essential in wound healing progression for the provision of oxygen and nutrients to the associated fibroblasts and for the transportation of blood-borne precursor cells to the healing area (30). To this point, the upregulation of Pecam1 (CD31) just happens to demonstrate the abundant formation of blood vessels and correlates with the result of the HE staining. By contrast, the lower expression of Cxcl14, a potent inhibitor of angiogenesis based on its ability to inhibit endothelial cell chemotaxis, is likely to facilitate neovascularization as well (31). Apart from them, two upregulated growth factor-like molecules, Areg and Cthrc1 (Collagen triple helix repeat-containing protein 1), also have the high potential to correlate with angiogenesis and cell migration. For example, Cthrc1 can trigger Wnt signaling, which in turn induces subsequent angiogenic program or promotes migratory ability (32,33). Areg belongs to the epidermal growth factor family and

is able to mediate transforming growth factor-β-induced pulmonary fibrosis (34). There is also evidence showing that Areg stimulates cell proliferation and exerts a potent anti-apoptotic effects on isolated fibrogenic cells (35). Another associated candidate in Table IV, Adamts1, which encodes a secreted and matrix-associated zinc metalloendopeptidase, was found to promote shedding of the transmembrane precursors of Areg and activation of the epidermal growth factor pathway (36). Taken together, the present findings suggested that persistent activation of the aforementioned chemokines and growth factors may drive urinary bladder fibrogenesis through angiogenesis and cell migration.

In view of the aforementioned causes coupled to the deregulated wound healing process and excessive mRNA level for collagens, although no obvious occurrence of immune cells infiltration was confirmed, as well as collagen proteins accumulation, it was still concluded that the results of the DEGs clearly demonstrated the existence of fibrogenic actions at an early stage. These findings have important implications of the molecular mechanisms underlying ketamine-induced urinary bladder fibrosis and reveal novel targets for the future development of effective therapies.

Acknowledgements

The present study was supported by grants from the National Science Council of the Republic of China, Taiwan (no. NSC101-2320-B-415-002-MY3) and from Chiayi Christian Hospital, Taiwan (no. R102-17).

References

1. Domino EF, Chodoff P and Corssen G: Pharmacologic Effects of Ci-581, a new dissociative anesthetic, in man. Clin Pharmacol Ther 6: 279-291, 1965.
2. Shahani R, Streutker C, Dickson B and Stewart RJ: Ketamine-associated ulcerative cystitis: A new clinical entity. Urology 69: 810-812, 2007.
3. Chu PS, Kwok SC, Lam KM, Chu TY, Chan SW, Man CW, Ma WK, Chui KL, Yiu MK, Chan YC, *et al*: 'Street ketamine'-associated bladder dysfunction: A report of ten cases. Hong Kong Med J 13: 311-313, 2007.
4. Chu PS, Ma WK, Wong SC, Chu RW, Cheng CH, Wong S, Tse JM, Lau FL, Yiu MK and Man CW: The destruction of the lower urinary tract by ketamine abuse: A new syndrome? BJU Int 102: 1616-1622, 2008.
5. Chuang SM, Liu KM, Li YL, Jang MY, Lee HH, Wu WJ, Chang WC, Levin RM and Juan YS: Dual involvements of cyclooxygenase and nitric oxide synthase expressions in ketamine-induced ulcerative cystitis in rat bladder. Neurourol Urodyn 32: 1137-1143, 2013.
6. Yeung LY, Rudd JA, Lam WP, Mak YT and Yew DT: Mice are prone to kidney pathology after prolonged ketamine addiction. Toxicol Lett 191: 275-278, 2009.
7. Juan YS, Lee YL, Long CY, Wong JH, Jang MY, Lu JH, Wu WJ, Huang YS, Chang WC and Chuang SM: Translocation of NF-kB and expression of cyclooxygenase-2 are enhanced by ketamine-induced ulcerative cystitis in rat bladder. Am J Pathol 185: 2269-2285, 2015.
8. Meng E, Chang HY, Chang SY, Sun GH, Yu DS and Cha TL: Involvement of purinergic neurotransmission in ketamine induced bladder dysfunction. J Urol 186: 1134-1141, 2011.
9. Gu D, Huang J, Shan Z, Yin Y, Zheng S and Wu P: Effects of long-term ketamine administration on rat bladder protein levels: A proteomic investigation using two-dimensional difference gel electrophoresis system. Int J Urol 20: 1024-1031, 2013.
10. Sangkum P, Gokce A, Tan RB, Bouljihad M, Kim H, Mandava SH, Saleem SN, Lasker GF, Yafi FA, Abd Elmageed ZY, *et al*: Transforming growth factor-β1 induced urethral fibrosis in a rat model. J Urol 194: 820-827, 2015.
11. Shen CH, Wang ST, Lee YR, Liu SY, Li YZ, Wu JD, Chen YJ and Liu YW: Biological effect of ketamine in urothelial cell lines and global gene expression analysis in the bladders of ketamine-injected mice. Mol Med Rep 11: 887-895, 2015.
12. Tsai TH, Cha TL, Lin CM, Tsao CW, Tang SH, Chuang FP, Wu ST, Sun GH, Yu DS and Chang SY: Ketamine-associated bladder dysfunction. Int J Urol 16: 826-829, 2009.
13. Veilleux-Lemieux D, Castel A, Carrier D, Beaudry F and Vachon P: Pharmacokinetics of ketamine and xylazine in young and old Sprague-Dawley rats. J Am Assoc Lab Anim Sci 52: 567-570, 2013.
14. Wu CH, Huang MH, Wang SM, Lin CC and Liu RH: Gas chromatography-mass spectrometry analysis of ketamine and its metabolites-a comparative study on the utilization of different derivatization groups. J Chromatogr A 1157: 336-351, 2007.
15. Sugino Y, Kanematsu A, Hayashi Y, Haga H, Yoshimura N, Yoshimura K and Ogawa O: Voided stain on paper method for analysis of mouse urination. Neurourol Urodyn 27: 548-552, 2008.
16. Deveaud CM, Macarak EJ, Kucich U, Ewalt DH, Abrams WR and Howard PS: Molecular analysis of collagens in bladder fibrosis. J Urol 160: 1518-1527, 1998.
17. Corazza O, Assi S and Schifano F: From 'Special K' to 'Special M': The evolution of the recreational use of ketamine and methoxetamine. CNS Neurosci Ther 19: 454-460, 2013.
18. Reyes-Gordillo K, Shah R, Arellanes-Robledo J, Hernández-Nazara Z, Rincón-Sánchez AR, Inagaki Y, Rojkind M and Lakshman MR: Mechanisms of action of acetaldehyde in the up-regulation of the human α2(I) collagen gene in hepatic stellate cells: Key roles of Ski, SMAD3, SMAD4, and SMAD7. Am J Pathol 184: 1458-1467, 2014.
19. Wong L, Hutson PR and Bushman W: Prostatic inflammation induces fibrosis in a mouse model of chronic bacterial infection. PloS One 9: e100770, 2014.
20. Stadelmann WK, Digenis AG and Tobin GR: Physiology and healing dynamics of chronic cutaneous wounds. Am J Surg 176 (Suppl 2A): S26-S38, 1998.
21. Broughton G II, Janis JE and Attinger CE: The basic science of wound healing. Plast Reconstr Surg 117 (Suppl 7): S12-S34, 2006.
22. Zeisberg M and Kalluri R: Cellular mechanisms of tissue fibrosis. 1. Common and organ-specific mechanisms associated with tissue fibrosis. Am J Physiol Cell Physiol 304: C216-C225, 2013.
23. Seki E, de Minicis S, Inokuchi S, Taura K, Miyai K, van Rooijen N, Schwabe RF and Brenner DA: CCR2 promotes hepatic fibrosis in mice. Hepatology 50: 185-197, 2009.
24. Moore BB, Kolodsick JE, Thannickal VJ, Cooke K, Moore TA, Hogaboam C, Wilke CA and Toews GB: CCR2-mediated recruitment of fibrocytes to the alveolar space after fibrotic injury. Am J Pathol 166: 675-684, 2005.
25. Ong VH, Carulli MT, Xu S, Khan K, Lindahl G, Abraham DJ and Denton CP: Cross-talk between MCP-3 and TGFbeta promotes fibroblast collagen biosynthesis. Exp Cell Res 315: 151-161, 2009.
26. Graham GJ and Locati M: Regulation of the immune and inflammatory responses by the 'atypical' chemokine receptor D6. J Pathol 229: 168-175, 2013.
27. Shi-Wen X, Rodríguez-Pascual F, Lamas S, Holmes A, Howat S, Pearson JD, Dashwood MR, du Bois RM, Denton CP, Black CM, *et al*: Constitutive ALK5-independent c-Jun N-terminal kinase activation contributes to endothelin-1 overexpression in pulmonary fibrosis: Evidence of an autocrine endothelin loop operating through the endothelin A and B receptors. Mol Cell Biol 26: 5518-5527, 2006.
28. Swigris JJ and Brown KK: The role of endothelin-1 in the pathogenesis of idiopathic pulmonary fibrosis. BioDrugs 24: 49-54, 2010.
29. Krönke G, Reich N, Scholtysek C, Akhmetshina A, Uderhardt S, Zerr P, Palumbo K, Lang V, Dees C, Distler O, *et al*: The 12/15-lipoxygenase pathway counteracts fibroblast activation and experimental fibrosis. Ann Rheum Dis 71: 1081-1087, 2012.
30. Tonnesen MG, Feng X and Clark RA: Angiogenesis in wound healing. J Investig Dermatol Symp Proc 5: 40-46, 2000.
31. Shellenberger TD, Wang M, Gujrati M, Jayakumar A, Strieter RM, Burdick MD, Ioannides CG, Efferson CL, El-Naggar AK, Roberts D, *et al*: BRAK/CXCL14 is a potent inhibitor of angiogenesis and a chemotactic factor for immature dendritic cells. Cancer Res 64: 8262-8270, 2004.

32. Ye X, Wang Y, Cahill H, Yu M, Badea TC, Smallwood PM, Peachey NS and Nathans J: Norrin, frizzled-4, and Lrp5 signaling in endothelial cells controls a genetic program for retinal vascularization. Cell 139: 285-298, 2009.
33. Ma MZ, Zhuang C, Yang XM, Zhang ZZ, Ma H, Zhang WM, You H, Qin W, Gu J, Yang S, *et al*: CTHRC1 acts as a prognostic factor and promotes invasiveness of gastrointestinal stromal tumors by activating Wnt/PCP-Rho signaling. Neoplasia 16: 265-278, 278.e1-e13, 2014.
34. Zhou Y, Lee JY, Lee CM, Cho WK, Kang MJ, Koff JL, Yoon PO, Chae J, Park HO, Elias JA and Lee CG: Amphiregulin, an epidermal growth factor receptor ligand, plays an essential role in the pathogenesis of transforming growth factor-β-induced pulmonary fibrosis. J Biol Chem 287: 41991-42000, 2012.
35. Perugorria MJ, Latasa MU, Nicou A, Cartagena-Lirola H, Castillo J, Goñi S, Vespasiani-Gentilucci U, Zagami MG, Lotersztajn S, Prieto J, *et al*: The epidermal growth factor receptor ligand amphiregulin participates in the development of mouse liver fibrosis. Hepatology 48: 1251-1261, 2008.
36. Liu YJ, Xu Y and Yu Q: Full-length ADAMTS-1 and the ADAMTS-1 fragments display pro- and antimetastatic activity, respectively. Oncogene 25: 2452-2467, 2006.